Compact Readout Electronics for Position Sensitive Photomultiplier Tubes

Peter Demetri Olcott, Jonathon A. Talcott, *Student Member, IEEE*, Craig Steven Levin, *Member, IEEE*, Frezghi Habte, *Member, IEEE*, and Angela M. K. Foudray, *Student Member, IEEE*

***Abstract*—Two charge multiplexed readout schemes for position-sensitive photomultiplier tubes (PSPMTs) have been developed and evaluated. A two-stage split-charge method is compared to standard positional charge division. The resulting electronic circuits are highly compact and will be initially incorporated into a hand-held gamma ray imager for cancer staging. Electrical tests on the readout electronics are performed and intrinsic scintillation camera performance is evaluated using a 23×23 array of pixilated $2 \times 2 \times 3$ mm^3 LSO crystals coupled to a H8500 flat-panel PSPMT.**

I. Introduction

POSITION-SENSITIVE photomultiplier tubes (PSPMTs) convert scintillation light into a high gain current signal localized to group of anode segments. The current signal distribution contains important information regarding the energy, timing, and location of gamma ray interactions in the scintillation camera, which can be useful in both high resolution SPECT and PET applications. In this work, compact PSPMT electronics are designed, built and tested for a hand-held gamma camera for cancer staging [1]. The H8500 PSPMT has a 25 cm^2 field of view (FOV) using 8×8 anodes on a 6 mm pitch. It is challenging to multiplex a large number of anode analog signals into a practical imaging system [2].

In this work we use a compact flat-panel PSPMT (Hamamatsu H8500) and a lutetium oxyorthosilicate:Ce (LSO) scintillation crystal array for imaging low energy single photon emitters [3]. The choice of LSO as a scintillation crystal in a collimated gamma camera possibly creates the condition where the inherit background that can contribute significantly to the measured activity. However, for $>90\%$ intrinsic detection efficiency for 140 keV photons only $\sim$3 mm thick LSO crystal is needed. For the 5×5 cm^2 camera field of view of interest, we use a 23×23 array of $2 \times 2 \times 3$ mm^3 LSO scintillation crystal pixels with a total LSO volume of roughly $50 \times 50 \times 3$ mm^3. Thus, with this relatively small LSO volume, a narrow energy window around 140 keV, and a high sensitivity collimator, the LSO background is not a significant problem.

The goal of this paper is to present the design and performance of a novel readout technique for the 8×8 array of 6×6 mm^2 PSPMT anodes which combines two compatible charge-multiplexed position-sensing techniques and compare the performance to more standard resistive charge division readout circuit.

Manuscript received November 15, 2003; revised October 11, 2004. This work was supported by Research Grant RG-01-0492 from the Whitaker Foundation.

P. D. Olcott, C. S. Levin, F. Habte, and A. M. K. Foudray are with the Department of Radiology and Molecular Imaging Program, Stanford University School of Medicine, Stanford, CA 94305 (e-mail: pdo@stanford.edu; cslevin@stanford.edu; fhabte@stanford.edu; afoudray@stanford.edu).

J. A. Talcott is with University of California, San Diego, CA USA (e-mail: jtalcott@ucsd.edu).

Digital Object Identifier 10.1109/TNS.2004.843134

II. Materials and Methods

A. Discretized Positioning Circuit (DPC)

Discretized position-sensitive readout circuits (DPC) [4] consist of a string or array of resistors that divide the charge between low impedance collection op-amps. The simple technique described provides positional charge division (Fig. 1). The X and Y position can be determined by (1)–(2)

$$X_{\text{position}} = \frac{(V_a + V_b) - (V_c + V_d)}{V_a + V_c + V_b + V_d} \tag{1}$$

$$Y_{\text{position}} = \frac{(V_a + V_d) - (V_c + V_b)}{V_a + V_c + V_b + V_d}. \tag{2}$$

B. Symmetric Charge Division (SCD) Circuit

Instead of summing all the charge into a large resistive division network, a novel technique of dividing the charge into an X and Y decoder network is used [5]. The incoming charge is split in half, with one part being collected in a X collection op-amp, and the other half in a Y collection op-amp (Fig. 1).

This novel technique which we will refer to as symmetric charge division (SCD) requires 16 amplifiers to collect the charge, one for each of the X rows and Y columns. For the H8500 flat-panel PSPMT, the position is encoded by determining the center of mass among the 8 channels along each row or column direction. The mismatch of charge deposited between X and Y paths are independent of each other. The drawback of this scheme is that it requires $2 * \sqrt{\text{N}}$ charge sensing preamplifiers for N anodes.

A standard and very robust and technique [6], [10] is used to reduce the number of channels from 16 to 4 by encoding the position along the axis as a current proportional to position (Fig. 1). Because charge sensitive preamplifiers are used, a low impedance voltage is available. The voltage can be converted to a position by using a resistive division network. This method is superior to conventional resistive charge division (Fig. 1) because amplification is performed before positional division. The amplified signal is robust enough to divide into a current signal proportional to position

$$R_{\text{row}} = \frac{R_m}{\left[\frac{(n_{\text{row}}-1)*(Gain-1)}{(N_{\text{channels}}-1)} + 1\right]}. \tag{3}$$

0018-9499/$20.00 © 2005 IEEE

Authorized licensed use limited to: Stanford University. Downloaded on May 25,2010 at 17:40:12 UTC from IEEE Xplore. Restrictions apply.

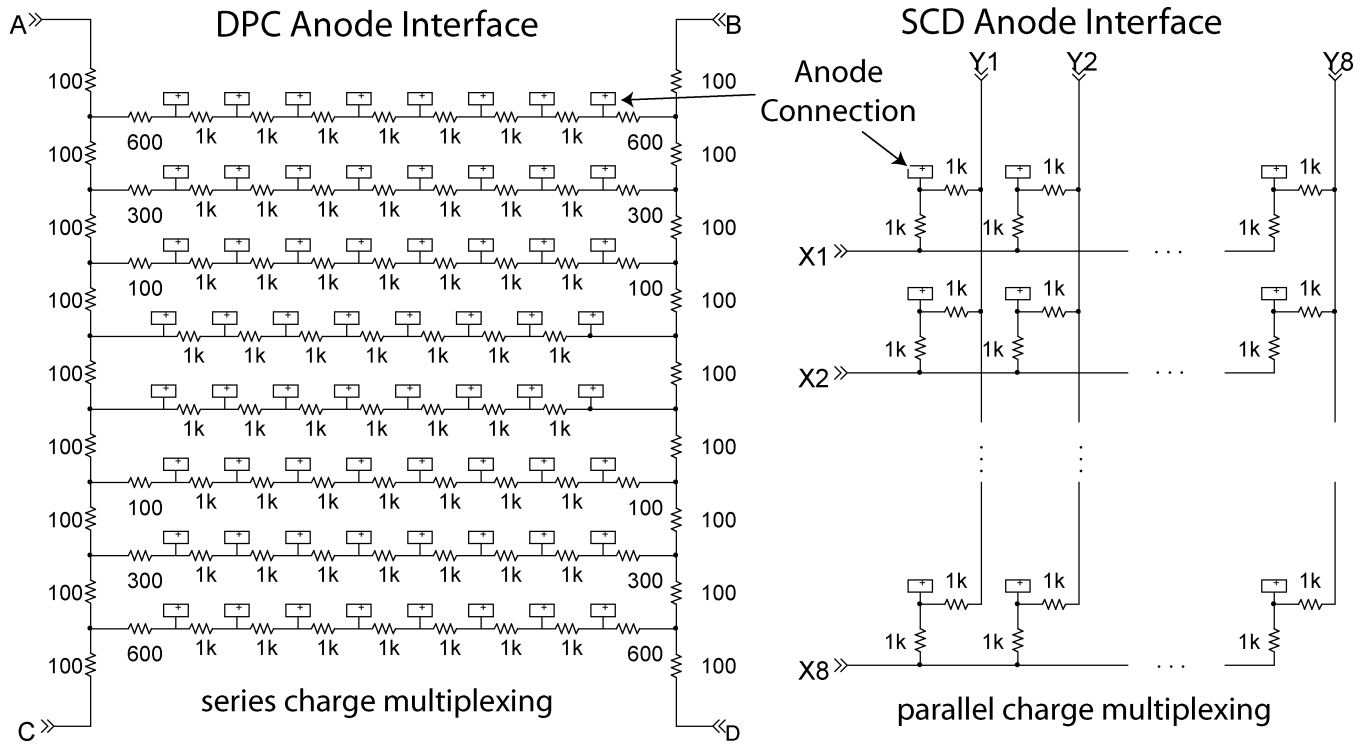

(a) (b)

Fig. 1. (a) Conventional two-dimensional (2-D) DPC network splits charge proportional to its Cartesian coordinates [9]. This charge is collected on 4 charge sensitive preamplifiers named A, B, C, and D. (b) SCD anode interface presents constant impedance to the anode, dividing the charge into equal buckets of charge for collection on a ROW and COLUMN preamplifier.

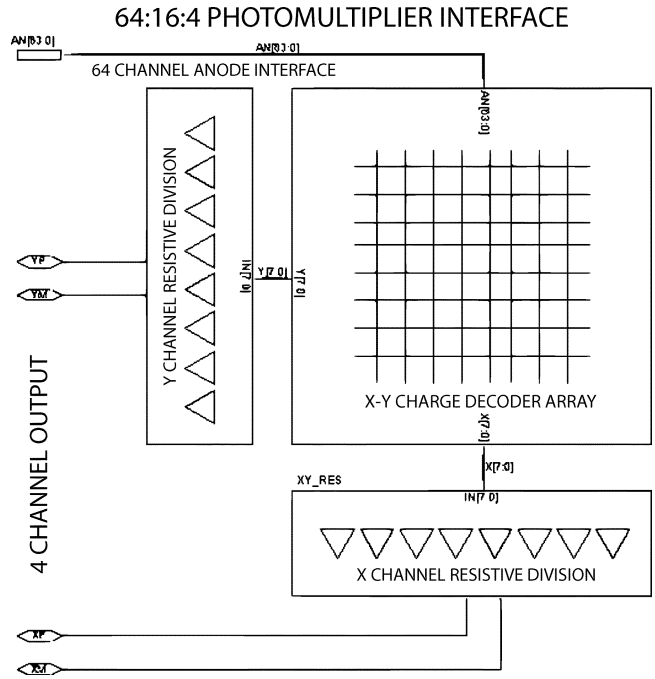

Fig. 2. Block diagram of newly proposed multi-anode interface.

The resistance on a row, R_{row} is determined by (3), where the readout scheme weights each resistor proportional to its position on the axis. Gain is the amount of small signal gain from the output of the first level preamp. $\mathrm{n_{row}}$ is the index of the of row,

TABLE I
SUMMARY OF SPATIAL LINEARITY PERFORMANCE

Readout	RMS Differential Linearity	RMS Noise in LSB	Peak-to-min Ratio
DPC	0.48%	3.3	27.3
SCD	0.62%	6.2	5.12

and $\mathrm{N_{channels}}$ is the total number of channels per axis, in this case 8

$$X = \frac{X_+ - X_-}{X_+ + X_-} \tag{4}$$

$$Y = \frac{Y_+ - Y_-}{Y_+ + Y_-}. \tag{5}$$

After the two charge splitting stages, the final position of an event is determined by (4) and (5). Fig. 2 shows a block diagram of the entire readout scheme proposed.

Comparing the position (4) and (5) to (1) and (2), we see that in the former the two output channels that encode x axis are independent of the y axis and vice-versa. Also, the maximum voltage differences between any channel compared to the other three is smaller in the proposed readout circuit. For example, if charge is injected in the corner of the resistor array, for the conventional design (Fig. 1), this maximum voltage was measured to be approximately 27 times larger than the minimum. On the other hand, in the proposed SCD design (Fig. 1), the peak voltage for an event on the corner was measured to be only approximately 5 times larger than the minimum (Table I). Both designs were analyzed with PSPICE before fabrication.

Authorized licensed use limited to: Stanford University. Downloaded on May 25,2010 at 17:40:12 UTC from IEEE Xplore. Restrictions apply.

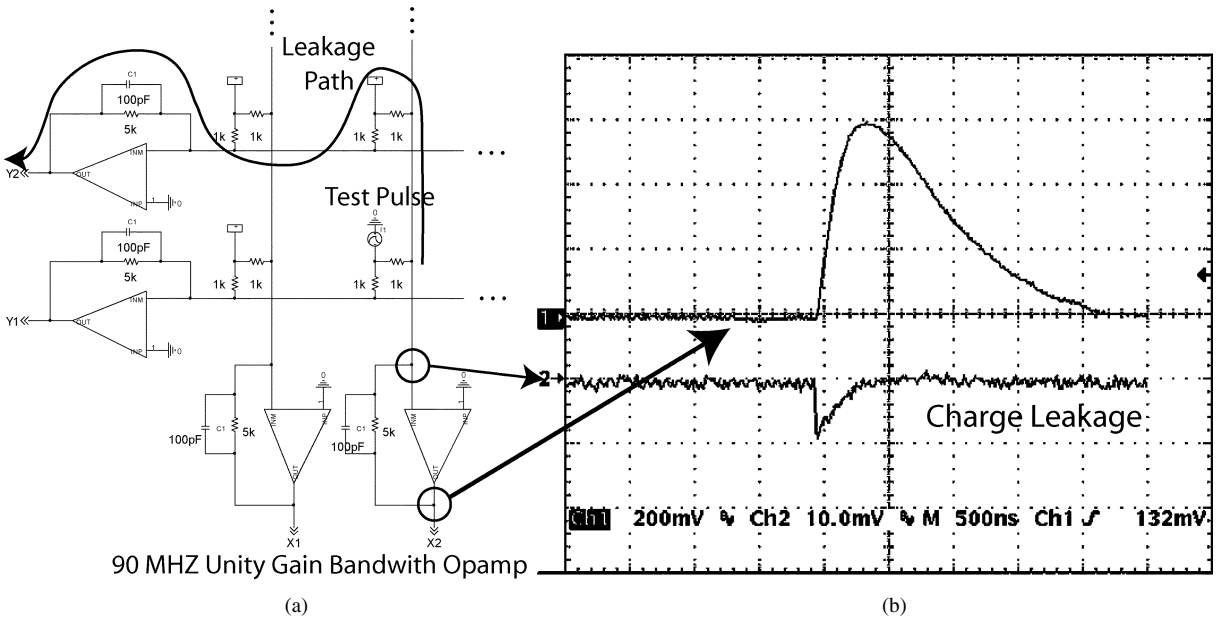

(a) (b)

Fig. 3. (a) Charge loss path exists from the anode to the virtual ground of the charge sensing preamp. In the example shown, a charge source, I8, injects charge that is split symmetrically and collected by an x axis and y axis preamp. Fourteen other anodes are connected to the same virtual ground and provide a path for charge to "leak." (b) In the scope measurement, the top trace corresponds to the op-amp output in response to a test pulse of current. The bottom trace is the measured voltage at the virtual ground.

III. Results

A. Charge Loss Mechanism

There exists a path in the symmetric charge decoder for charge to be lost (Fig. 3). First, the analysis of the impedance of virtual ground is critical in understanding this design limitation. An op-amp, with an inverting feedback network that comprises a capacitor C and resistor R in parallel with the total Z dominated by the capacitor C, operates as a charge sensing preamplifier. The time dependent output voltage, $V_{\rm out}$, in response to an impulse of current $Q_{\rm in}$ in the proposed circuit can be expressed as in (6)

$$V_{out}(t) \approx -\frac{Q_{in}}{C}\left(e^{-\frac{t}{RC}}\right). \tag{6}$$

The parallel combination of R and C can be expressed as the impedance Z. The impedance, as a function of ω (frequency) looking into the virtual ground with an amplifier with input resistance $R_{\rm in}$, finite gain A_0 and bandwidth ω_0 is given by (7)

$$R_{in}(\omega) \approx \frac{\|Z\|}{\sqrt{\left[1+\frac{A_0^2}{1+\frac{\omega^2}{\omega_0^2}}\right]}}. \tag{7}$$

Because of thermal issues due to power consumption of the op-amp, the gain A_0 and bandwidth ω_0 to cannot be fully optimized to minimize $R_{\rm in}$. The 7 resistors and PSPMT anodes connected to each op-amp virtual ground (Fig. 3) form a parasitic path. Because a PSPMT anode is very close to an ideal current source, the charge splitting resistors connect all of the preamp virtual grounds to each other. The charge from the anode after symmetric division is further divided by finite impedance, $R_{\rm in}$, and the parasitic impedances of the other 7 preamps in a series combination of two charge splitting resistors with the finite impedances of the parasitic op-amps. The value of the charge splitting resistors must be large compared to effective $R_{\rm in}$ of the charge sensing preamp otherwise a large amount of charge will be lost, creating an offset voltage on unrelated preamps (see Fig. 3).

B. Noise Analysis

Due to the 2-D nature of the calculated x and y position, noise is calculated as variation in distance from the calculated mean point of an event distribution in the x-y plane. The quantization range of the ADC puts a lower floor on the variation in position, expressed as a least significant bit (LSB). Distances in our noise analysis are normalized to LSB units. The digital acquisition system used for both readout schemes was a National Instruments 4-channel 12-bit simultaneous sampling ADC. As shown in Table I, the DPC readout has a lower output referred noise floor than the SCD readout. The SCD readout has 16 preamplifiers each contributing their own noise to the output. By contrast, the DPC readout with only 4 preamplifiers contributes 4 times less noise, or 2 times less RMS noise (because the noise is uncorrelated). Schemes exist to remove the added noise of the preamplifiers by using a technique of a threshold preamplifier [6]. A threshold preamplifier will not amplify any signal unless a predetermined input threshold has been crossed. Using this technique can significantly reduce the noise of the nonactive preamplifiers.

C. Electrical Spatial Linearity

To obtain spatial response using (1)–(4) for the DPC and PCD circuits, the four coaxial outputs of the front-end electronics are coupled to four spectroscopy amplifiers and a trigger system for use with a four-channel 12-bit 100 ksps ADC board. The spectroscopy amplifiers perform Gaussian shaping with a 500

Authorized licensed use limited to: Stanford University. Downloaded on May 25,2010 at 17:40:12 UTC from IEEE Xplore. Restrictions apply.

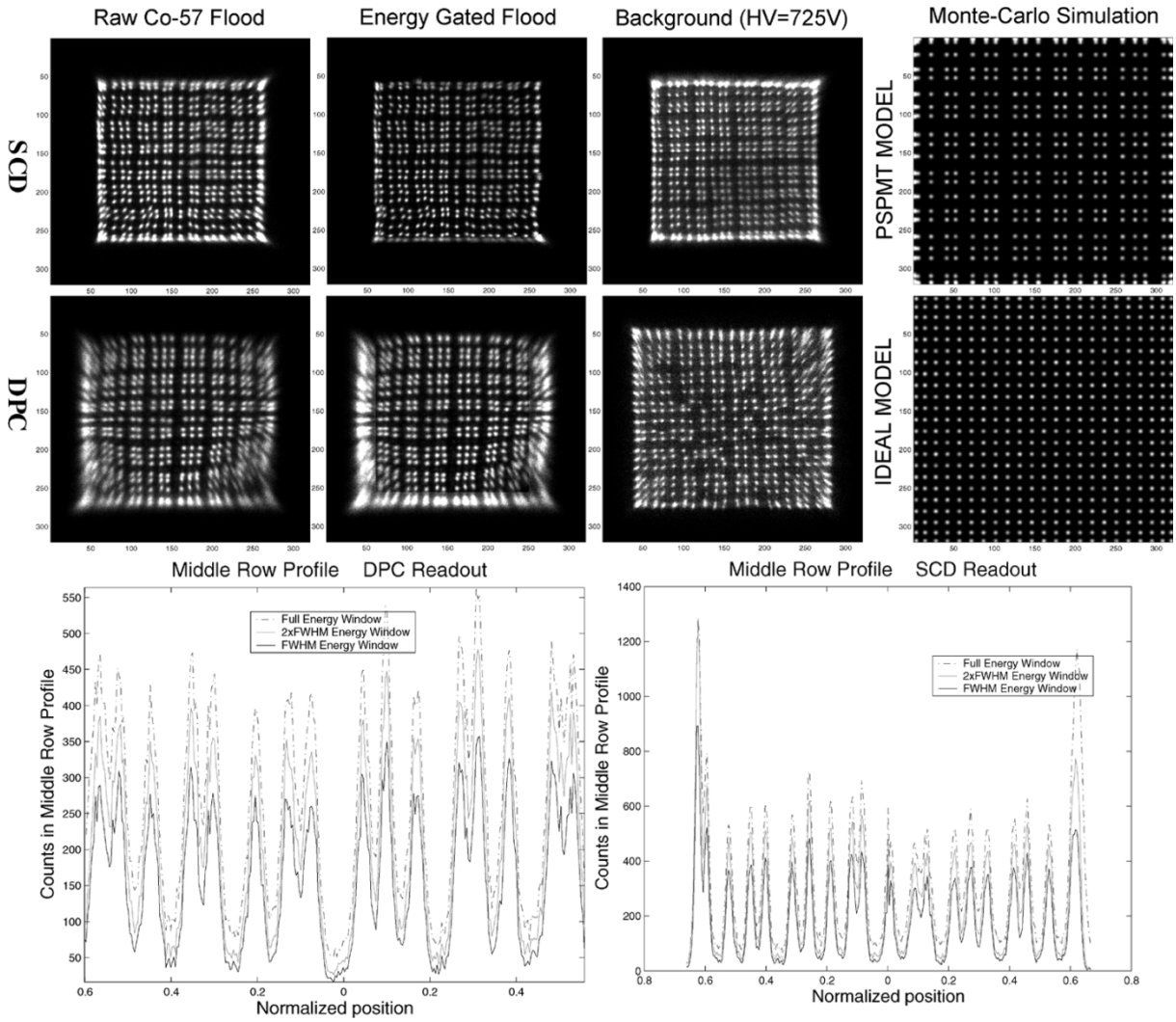

Fig. 4. Flood histogram performance for the SCD readout (top row right) and DPC readout (middle row right) and their corresponding middle row profiles (bottom) Raw flood data with open energy window (left column) is compared for the central field-of-view of the image with the data using a 2σ energy gating around the 122 keV photopeak (middle column). Gray scale threshold is set high to emphasize light distribution. Comparison of ^{176}Lu background images acquired with a PSPMT bias voltage at 725 V (versus 1000 V) shows a drastic improvement in spatial linearity for the DPC readout (right column). Middle row profiles with and without a 2σ energy gating, only for resolved crystals, are shown for the DPC readout (left, bottom) and SCD readout (right, bottom). Monte Carlo results are presented with an ideal position sensitive detector (right bottom) and PSPMT anode dead zone (right top). The 2 million event Monte-Carlo results were blurred with a 10×10 Gaussian filter to account for several ideal assumptions.

ns time constant. The 500 ns time constant is not optimal for the 40 ns decay constant of LSO. Both charge-multiplexed designs (DPC and SCD) were electrically probed to determine spatial linearity. The electrical probe consisted of a RC network designed to emulate the amount of charge and decay characteristics of an LSO pulse. An approximate 100 pC charge impulse with 40 ns exponential decay time constant was used to test the entire positioning chain within both readout configurations. Comparing diagonal middle row linearity, each design performed within the tolerances of the passive components used and estimated by PSPICE Monte-Carlo simulations of the designs before fabrication

Both designs showed excellent diagonal spatial linearity of less than 1% (see Table I). The DPC design performs slightly better due to the use of matched equal valued resistors. The SCD design is forced to use precise nonmatched 1% resistors with a value based on (3).

D. Flood Histogram Performance

The readout electronics plus the acquisition system were attached to the PSPMT coupled to a 23×23 array of $2\times2\times3$ mm^3 LSO scintillation crystals. The crystals were polished on the one small face coupled to the PSPMT and the other faces of each crystal were "as cut." Each crystal was individually wrapped in two layers of white diffusely reflecting Teflon tape and then packed into the 23×23 array. The backside of the entire array was coated with 4 more Teflon layers. The crystal array was directly coupled to the 2 mm thick glass window of the PSPMT without any additional light diffuser or coupling grease. The PSPMT has 49 mm $\times$ 49 mm of sensitive area. The 23×23 crystal array measured 50 mm $\times$ 50 mm with approximately a 2.1 mm pitch in each direction. Thus, each of the crystals on the array perimeter had only roughly one quarter of their area coupled to the sensitive area of the PSPMT. Due to the small volume of the $2 \times 2 \times 3$ mm^3 LSO crystals, the total measured

Authorized licensed use limited to: Stanford University. Downloaded on May 25,2010 at 17:40:12 UTC from IEEE Xplore. Restrictions apply.

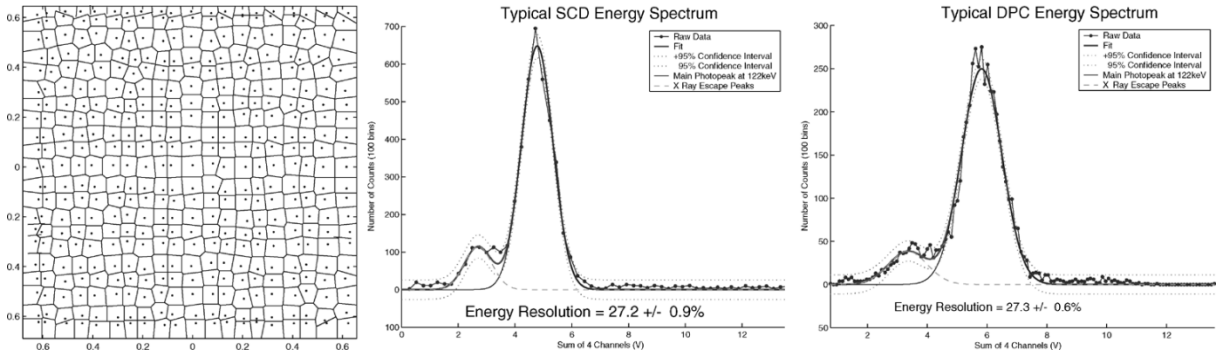

(a) (b)

Fig. 5. (a) SCD crystal map is generated using Gaussian blurring followed by nonmaximal suppression to generate a table of peaks. Events are binned based on the minimum distance to a peak. (b) Example energy spectra for two individual crystals extracted from a flood irradiation by $^{57}\mathrm{Co}$. Photopeak for $^{57}\mathrm{Co}$ is 122 keV with a lutetium K-shell x-ray escape peak at ~59 keV (122 keV − 63 keV).

background from $^{176}\mathrm{Lu}$ was only ~400 cps for the 529 crystals (~0.76 cps/crystal) in a broad energy window from 50–400 keV. If a FWHM (~26%) energy window at 140 keV is used instead, then the number of background counts would go down by a factor of ~12.5 to ~32 cps, allowing the use of this small volume of LSO.

E. Monte Carlo Simulation

The scintillation array and the PSPMT were simulated using custom gamma ray transport code and followed by a light transport model [4]. This simulation can predict imaging performance of the gamma ray detector module. Because each photon is traced and recorded, the detector nonlinearities can be modeled. In Fig. 4, the 2 million event Monte-Carlo simulation correctly predicts the total number of resolved crystals and also the positioning nonlinearity of the PSPMT. Measured data and simulation resolve ~ 21 × 21 crystals. The anode pitch and surrounding dead area relative to the array crystals creates the observed nonlinearity in the flood histogram and makes it difficult to position crystals at the edge of the array. The current model does not account for the variation in the number of photons created per eV for each gamma ray interaction, variation in the quantum efficiency of the PMT photocathode, variation in the dynode amplification of electrons generated from the PMT, and electrical readout noise and quantization effects. All these effects were lumped into a single empirical Gaussian blurring factor.

F. Flood Irradiation

The array was flooded by a 100 μC $^{57}\mathrm{Co}$ source at approximated 10 cm from the center of the array. Approximately 1.9×10^4 events per second interacted with the crystal array and were collected by the acquisition system (Fig. 4). Both readout schemes (DPC and SCD) were not able to resolve all 23 × 23 crystals in the array. For example, along the middle row profiles shown in Fig. 4 both schemes were only able to resolve 21 crystals. More than one crystal on each side mapped to the same single anode row/column location creating a hot edge artifact. This can be clearly seen in Fig. 4 on the edges of the middle row profile of the SCD readout and around the perimeter of the raw flood images, and also in the Monte-Carlo simulation (Fig. 4). When 2-sigma energy gating is used, this extra row can be clearly distinguished in the profile. The DPC readout shows significant barrel distortion in the flood irradiation versus the background image. The preamp configuration

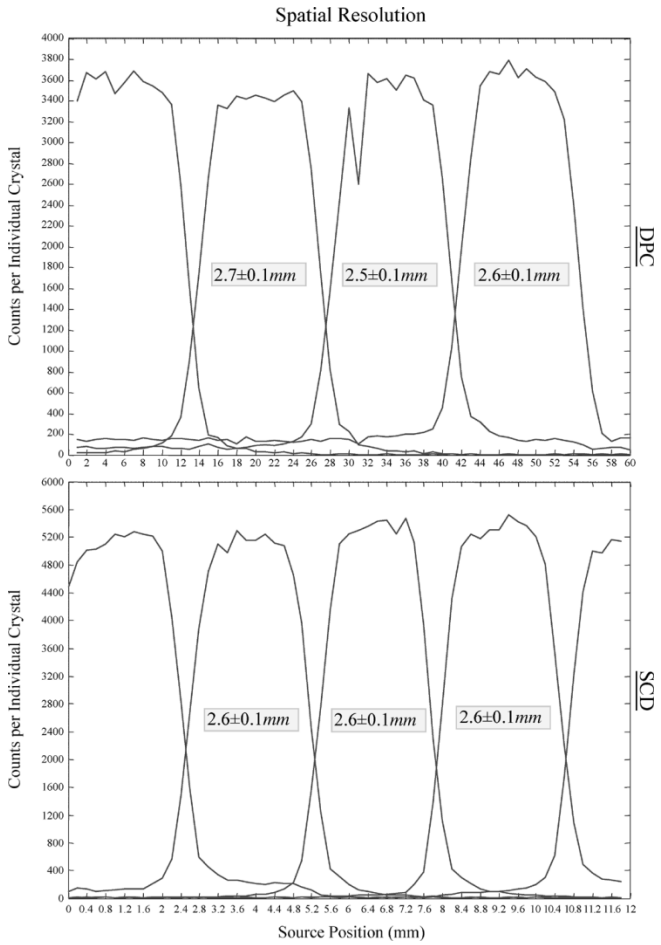

Fig. 6. Spatial resolution measured for DPC (top) and SCD (bottom) readouts with a collimated source that is stepped across array at 200 um intervals with a 0.7 mm spot size for a fixed time interval. Counts are acquired as a function of source position and binned to individual crystals with energy gating at the FWHM energy resolution. FWHM spatial resolutions are measured as trapezoids fitted to the crystal profiles. As can be seen, background radioactivity was low and so was not subtracted for these measurements.

Authorized licensed use limited to: Stanford University. Downloaded on May 25,2010 at 17:40:12 UTC from IEEE Xplore. Restrictions apply.

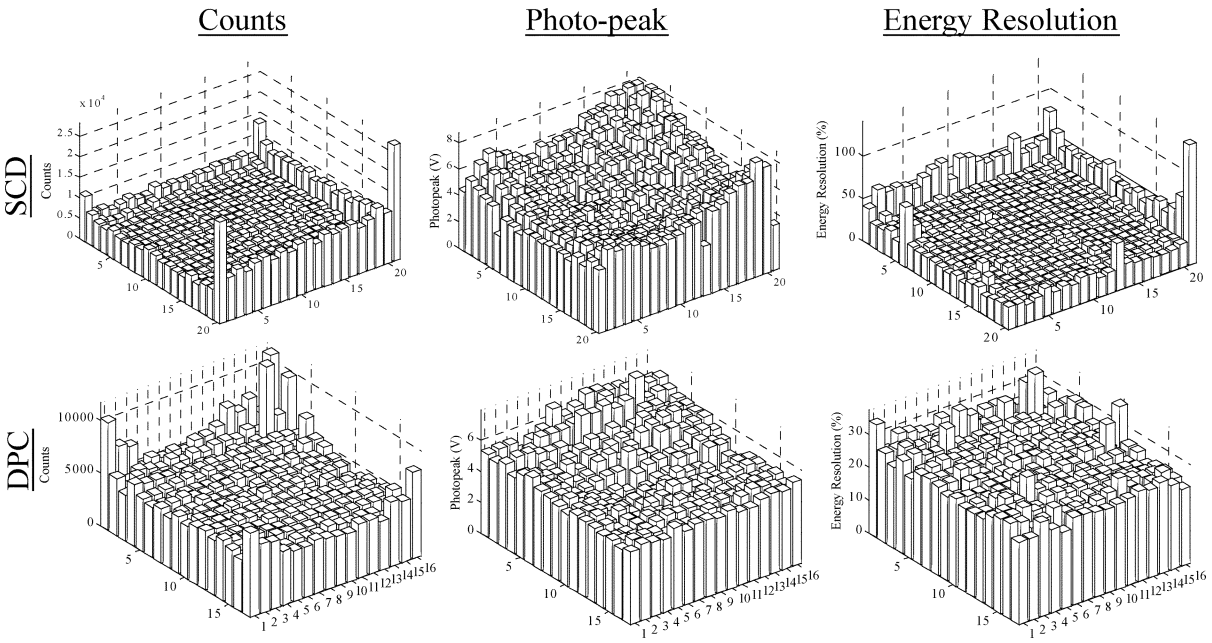

Fig. 7. Individual crystal statistics for counts (left), photo-peak mean (middle), and energy resolution (right) for SCD (top) and DPC (bottom) readouts for raw flood data (no energy gating). Events are binned to individual crystals based on the minimum distance to an identified peak. Peaks are calculated using a blurring filter followed by nonmaximal suppression to better approximate the center of mass. The SCD statistics were calculated for 20 × 21 crystals, whereas due to edge nonlinearity, the DPC imager data is only for the inner 17 × 16 crystals. The total number of crystals in the physical array was 23 × 23.

of the DPC electronics used the same feedback networks as the SCD design. The large peak-to-min voltage ratio for the DPC readout put much larger signals in the corners and edges than the gain and bandwidth supported. The distortion is not present in the background image (Fig. 4) because the high voltage supply was reduced to a level where peak-to-min pulse height ratios were reduced and spatial linearity was recovered. Unfortunately at 750 V PSPMT bias, the low energy $^{57}\mathrm{Co}$ spectrum is not within the dynamic range of the acquisition system, and only the high-energy tails of the $^{176}\mathrm{Lu}$ background could be imaged.

G. Spatial Resolution

Both readouts performed well in resolving the $2\times2\times3$ mm^3 LSO array crystals spaced at ∼2.1 mm pitch. Spatial resolution was determined by the convolution between the spot size (0.7 mm) and the rectangular crystal size (2.0 mm) to about 2.6 mm (Fig. 6). Due to the small size of the crystal gamma ray scattering has little affect on the spatial resolution. Crystal-to-crystal scatter would involve such large Compton angles as to be rejected by energy gating. Other energy escape modes involving the loss of a lutetium K-shell x-ray, Auger electron, or an ejected photoelectron also would have large measurable energy loss that would be removed by energy discrimination.

H. Individual Crystal Statistics

Crystals were extracted from the flood irradiation list mode data and analyzed on a crystal-by-crystal basis according to a crystal map (Fig. 5). Two-dimensional bar plots as a function of crystal location within the array capture the counts that fall within a crystal location, mean photopeak pulse height, and the energy resolution (Fig. 7).

TABLE II
ENERGY RESOLUTION COMPARISON

Readout	Best Resolution	Average Resolution	Worst Resolution	Std Deviation
DPC	22.9%	27.0%	37.5%	2.1%
SCD	23.2%	26.9%	44.9%	1.0%

I. Energy Resolution

The ∼27% mean photopeak energy resolution value (Fig. 7 and Table II) at 122 keV compares with the energy resolution measured by others [3] for $^{99\mathrm{m}}\mathrm{Tc}$ (140 keV photo-peak) using $2\times2\times10$ mm^3 LSO crystals. The small size of the individual array crystals at $2\times2\times3$ mm^3, significant variation over the photocathode surface, and relatively large PSPMT anodes (5.6×5.6 mm^3) resulted in a large nonuniformity in the collected light energy. Fig. 5 shows a typical energy spectra for the two readouts for a single crystal by itself in the array. The small size of the crystals means that significant lutetium K-shell X-rays will escape, which explains the presence of the smaller low energy peak.

Energy resolutions extracted in Table II do not include edge crystals for the SCD and DPC readouts because the two designs had very different performance at the edges (SCD was superior). Therefore, the comparison is valid over the crystals that the two designs did resolve.

On average, the light from each event is shared among several anodes. Because each anode has a different gain, the variation in the anodes convolves with the light distribution to broaden the energy peak. To confirm that the crystal size effects energy resolution, a single much larger crystal with dimensions of $2\times3\times10$ mm^3 was coupled sideways (3×10 mm face) to the PSPMT; an energy resolution of $21.9+/-0.3\%$ was measured.

Authorized licensed use limited to: Stanford University. Downloaded on May 25,2010 at 17:40:12 UTC from IEEE Xplore. Restrictions apply.

Using single isolated crystals of $2 \times 2 \times 3$ mm^2 LSO did not improve the energy resolution by any significant factor compared to that measured from individual crystals of an array, ruling out the possibility that light sharing or other crystal array artifacts have any significant effect on the measured energy resolution.

Compared to NaI(Tl)-based scintillation cameras, LSO has a poor energy resolution ($\sim$27%) that can be attributed to the to lower the number of photons produced per MeV of interaction. The excess energy resolution degradation for LSO not related to counting statistics (number of photons per MeV) is not fully understood but may be related to the nonproportionality of luminous efficiency versus electron energy [8].

J. Mean Photopeak Pulse Height

The variation of mean photopeak pulse height of DPC and SCD designs in Fig. 7 indicates that there is a relatively large nonuniformity in the amount of charge deposited over the anodes (mainly due to photocathode nonuniformity and relative dimensions between the crystal and anode pitch). Both readout techniques exhibit the effect that one corner is particularly "hot" compared to the other corners. This is most likely due to photocathode nonuniformity rather than variations in crystal light yield.

IV. Discussion

A direct comparison between both readout schemes cannot be fairly done due to the compression artifacts seen and measured in the flood histograms for the DPC readout. If the preamplifier gains are set correctly by choosing a different feedback network, the DPC readout spatial linearity measured from a ^{57}Co flood would be the same as seen for its background image in Fig. 4. While for this different DPC feedback network the spatial linearity would be restored since the peak-to-min pulse height ratio would decrease, a loss in signal amplification would degrade the energy resolution of the DPC readout. Where the two readout schemes do compare well is in the middle of the crystal array where compression artifacts are not present (Fig. 4 and Fig. 7). Here both readout schemes perform approximately the same in terms of count rate efficiency, photo-peak voltage, and energy resolution.

The true performance limit in this analysis is the scintillator crystal array. The scintillation array used in our experiments had a small light cone distribution per event due to the small size of the crystals ($2 \times 2 \times 3$ mm^3) and the lack of any light guide or optical grease. Because so many crystals are being light multiplexed over a single anode of the PSPMT at the edge, individual crystal locations cannot be separated, and several crystals merge. This scintillation crystal configuration produced a highly focused light cone seen by the PSPMT photo-cathode, but may have resulted in inadequate light spread over the 5.6 mm anodes to correctly position events at the center and especially the edge of the PSPMT. Edge crystals with too small of a light cone would deposit all their light into a single anode, which in turn would bias the positioning to the center of an anode piling up the calculated events.

V. Summary and Conclusion

We have developed and compared two compact charge multiplexing readout schemes for readout of a flat-panel PSPMT. Both readouts provide good spatial linearity and dynamic range, and good spatial and energy resolutions. Both readout schemes (DPC and SCD) can be further optimized to provide better energy resolution and crystal edge identification for this surgical held imager.

It is important to have a scintillation crystal array, which will focus light in such a way, that minimizes the variation in light distribution, and which allows edge crystals to be correctly positioned within the array. We are currently investigating NaI(Tl) arrays in hope that we can improve the spatial linearity but still maintain good energy resolution performance. The appropriate collimator will allow the complete hand-held gamma ray camera to be assembled. This camera will satisfy the requirement of compactness, flexibility, and high-resolution imaging performance for use as a 2-D surgical camera.

Finally, we are also exploring SCD readout electronics for the multiplexing an array of position sensitive avalanche photodiodes to replace the PSPMT.

Acknowledgment

The authors would like to acknowledge PCB Express (http://www.pcbexpress.com/) for their donation of services for the fabrication of the PCB board. We acknowledge Don Johnson at UCSD CRMS, for his help in the fabrication of the fixtures for the spatial measurement, V. Popov at Jefferson National Lab for very useful conversations related to the SCD readout, and Serge Belongie at UC San Diego for his help with the crystal segmentation algorithm.

References

[1] D. P. McElroy, E. J. Hoffman, and L. MacDonald *et al.*, "Evaluation of performance of dedicated, compact scintillation cameras," in *Proc. Nuclear Science Symp. Conf.*, vol. 3, Oct. 15–20, 2000, pp. 21/109–21/113.

[2] R. Pani, A. Soluri, and R. Scafe *et al.*, "Multi-PSPMT scintillation camera," *IEEE Trans. Nucl. Sci.*, vol. 46, no. 3, pp. 702–708, Jun. 1999.

[3] J. J. Vaquero, J. Seidel, and S. Siegel *et al.*, "Performance characteristics of a compact position-sensitive LSO detector module," *IEEE Trans. Med. Imag.*, vol. 17, no. 6, pp. 967–978, Dec. 1998.

[4] S. Siegel, S. R. Cherry, and Y. Shao, "Simple charge division readouts for imaging scintillator arrays using a multi-channel PMT," *IEEE Trans. Nucl. Sci.*, vol. 43, no. 3, Jun. 1996.

[5] V. Popov, "Matrix Output Device Readout System," United States Patent Office, #6 747 263, Jun. 2004.

[6] D. R. Rollo, *Nuclear Medicine Physics, Instrumentation, and Agents*. Saint Louis, MO: Mosby, 1977, pp. 232–237.

[7] C. Moisan, F. Cayouet, and G. McDonald, "DETECT2000: The object oriented C++ language version of DETECT: A program for modeling optical properties of scintillators," Dept. Electr. Comput. Eng., Laval Univ., Quebec City, QC, Canada.

[8] W. W. Moses, "Current trends in scintillator detectors and materials," *Nucl. Instrum. Methods Phys. Res.*, no. 487, pp. 123–128, 2002.

[9] W. W. Cherry *et al.*, "High resolution detector array for gamma-ray imaging," U.S. Patent #5 719 400, Feb. 1998.

[10] V. Popov, S. Majewski, A. G. Weisenberger, and R. Wojcik, "Analog readout system with charge division type output," in *Proc. Nuclear Science Symp. Conf. Rec.*, vol. 4, Nov. 2001, pp. 1937–1940.

Authorized licensed use limited to: Stanford University. Downloaded on May 25,2010 at 17:40:12 UTC from IEEE Xplore. Restrictions apply.